Turkish Journal of Electrical Engineering & Computer Sciences

http://journals.tubitak.gov.tr/elektrik/

Research Article

Turk J Elec Eng & Comp Sci
(2019) 27: 274 – 288

doi:10.3906/elk-1806-17

Improved VSM control of PMSG-based wind farms for transient stability enhancement

Mohamed ABBES[1,2,*], **Ines MEHOUACHI**[1,2], **Souad CHEBBI**[1,2]
[1]National School of Engineering of Tunis (ENSIT), University of Tunis, Tunis, Tunisia
[2]Laboratory of Technologies of Information, Communication, and Electrical Engineering (LaTICE), Tunis, Tunisia

Received: 02.06.2018 • **Accepted/Published Online:** 24.10.2018 • **Final Version:** 22.01.2019

Abstract: This paper analyzes the optimal control strategy of PMSG-based wind farms during faults in order to improve the transient stability of a power system with a high penetration rate of wind power. The investigated control strategies are the unity power factor (UPF), reactive power control (RPC), and particularly the concept of virtual synchronous machine (VSM). The transient stability level is assessed using the critical clearing time index, which was calculated based on trajectory sensitivity analysis. In light of the obtained results, it was found that RPC gives the best transient stability level, followed by the classical VSM control. Hence, an improved VSM control was proposed based on the transient model of a synchronous generator. The improved VSM has shown a behavior similar to a real synchronous generator, which results in better transient stability performances.

Key words: Transient stability, wind power, PMSG, critical clearing time, virtual synchronous generator

1. Introduction

According to the statistics of the International Renewable Energy Agency (IRENA) released in 2017, wind energy is one of the fastest-growing renewable sources since it has proved its effectiveness and its economic benefits [1]. However, large-scale integration of wind power represents a challenge for transmission system operators in terms of ensuring safe and stable operation of the electrical network [2]. Many research works have investigated the impact of high wind generation level on the stability of power systems. The influence of increased penetration of fixed speed wind systems was analyzed in [3–5]. In [6], the impact of integrated DFIGs on the transient dynamics of a power system was analyzed using the center of inertia (COI) approach. The impact of DFIG-based wind farms on transient and small signal stability was also discussed in [7] and [8]. In [9], the authors used sensitivity-based analysis to study the effect of DFIG-based wind farms on power system stability during voltage dips. In view of this literature review, it is noted that most of studies have dealt with the impact of SCIG-based wind farms and DFIG-based wind systems on the transient and small signal stability of the electrical network. For direct drive technology, a variety of control strategies have been proposed to manage the production of wind turbines during transient events. In [10], the authors analyzed their transient performances with two control modes, namely unity power factor and reactive power control. In [11], the virtual inertia control of PMSG-based wind systems was presented and analyzed. The virtual inertia approaches were classified into three categories: synchronization control, supplementary signals for frequency control, and the VSM. The concept of VSM aims to emulate the behavior of synchronous generators in order

*Correspondence: mohamed.abbes@esstt.rnu.tn

to stabilize the power system [12, 13]. It was applied in microgrids to control distributed generation sources [14, 15] and generation systems with short-term energy storage [16]. Thus, the objective of this work is to identify the best control method of PMSG-based wind farms in terms of transient stability enhancement. The obtained performances are also compared with the stability level when only real synchronous generators are used. For the different production scenarios, the trajectory sensitivity approach (TSA) was used to estimate the critical clearing time (CCT), which is considered as a stability index [17, 18]. In light of the obtained results, a modified VSM control is proposed in order to improve the transient behavior of variable speed wind farms. With the improved VSM control, the response of the wind farm becomes even closer to that of a real synchronous generator and the CCT is increased. The next section presents the power system modeling and aggregate model of the PMSG-based wind systems. Section 3 discusses the basic theory of trajectory sensitivity analysis. In the fourth section, the transient stability of the power system is assessed for different wind energy production scenarios and the best control strategy is identified. In Section five, an improved VSM is compared to the classical VSM and the SG in terms of transient stability improvement.

2. Power system modeling

This section presents the modeling of the two-area power system including the wind farm (Figure 1) . The power system is based on a 9-bus test system. Detailed parameters are listed in Table 1.

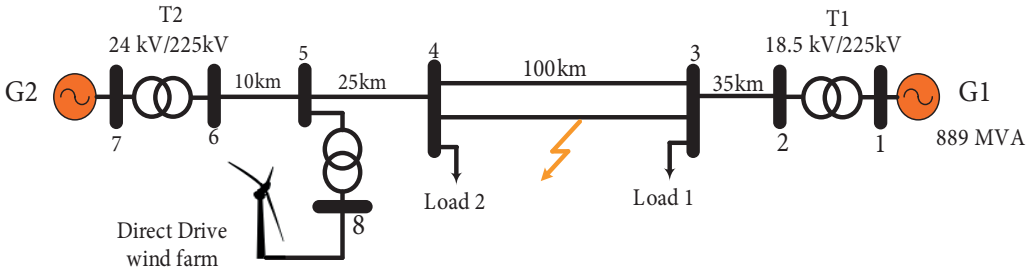

Figure 1. Schematic of the two-area power system including a wind generation system.

Table 1. Parameters of synchronous generators.

Parameter	Generator 1	Generator 2	Unit
Base power S_b	889	555	MVA
Base voltage (line-to-line)	18.5	24	kV
Poles pairs	2	2	-
Stator resistance R_s	0.003	0.003	p.u.
Synchronous reactance X_d	1.72	1.81	p.u.
Synchronous reactance X_q	1.69	1.76	p.u.
Transient reactance X'_d	0.36	0.3	p.u.
Transient reactance X'_q	0.4	0.25	p.u.
Time constant T'_{do}	5.7	8	s
Time constant T'_{qo}	0.04	0.07	s
Inertia H	6.3	4.3	s

2.1. Synchronous generators

The synchronous generators are represented by the simplified model 1.1, which neglects stator transients. This model assumes a field circuit on the d-axis and one equivalent damper on the q-axis [19]. A simplified model including one gain and one time constant is used to represent the excitation system. The generator and the exciter models are described by the following equations written in the p.u. system [20, 21]:

$$\frac{d\delta_i}{dt} = \omega_{r0}\Delta\omega_{r_i} \tag{1}$$

$$\frac{d\Delta\omega_{r_i}}{dt} = \frac{1}{2H_i}\left(-K_D\Delta\omega_{r_i} + T_{m_i} - T_{e_i}\right) \tag{2}$$

$$T^t_{do_i}\frac{dE^t_{q_i}}{dt} = \left[-\frac{X_{d_i}}{X^t_{d_i}}E^t_{q_i} + \left(\frac{X_{d_i}}{X^t_{d_i}} - 1\right)V_i\cos\left(\delta_i - \theta_i\right) + E_{fd_i}\right] \tag{3}$$

$$T^t_{qo_i}\frac{dE^t_{d_i}}{dt} = \left[-\frac{X_{q_i}}{X^t_{q_i}}E^t_{d_i} + \left(\frac{X_{q_i}}{X^t_{q_i}} - 1\right)V_i\sin\left(\delta_i - \theta_i\right)\right] \tag{4}$$

$$T_{A_i}\frac{dE_{fd_i}}{dt} = -E_{fd_i} + (V_{ref} - V_i)K_A \tag{5}$$

In the above equations, δ_i represents the rotor angular position and $\Delta\omega_{r_i}$ is the speed deviation with respect to the nominal speed ω_{r0}. H_i is the inertia constant and K_{D_i} is a load damping constant. T_{m_i} and T_{e_i} are respectively the mechanical and the electrical torques. X_{d_i} and X_{q_i} are the d-axis and q-axis synchronous reactance, while $X^t_{d_i}$ and $X^t_{q_i}$ are the transient reactance. $T^t_{do_i}$ and $T^t_{qo_i}$ are the time constants of rotor circuits, and T_{A_i} and K_{A_i} are the gain and time constant of the exciter. V_i is the magnitude of stator voltages and θ_i represents the angle of this voltage in the reference synchronous frame.

2.2. Network model

Transients associated to the electrical grid are neglected in stability studies since they decay very rapidly and their effect is insignificant [21]. Hence, the electrical grid is represented by a set of algebraic equations, given by:

$$P_{Bi} = \sum_{i=1}^{n}|V_i|\,|V_j|\left(G_{ij}\cos\left(\theta_i - \theta_j\right) + B_{ij}\sin\left(\theta_i - \theta_j\right)\right) \tag{6}$$

$$Q_{Bi} = \sum_{i=1}^{n}|V_i|\,|V_j|\left(G_{ij}\sin\left(\theta_i - \theta_j\right) - B_{ij}\cos\left(\theta_i - \theta_j\right)\right) \tag{7}$$

Here, G_{ij} and B_{ij} are respectively the real and the imaginary parts corresponding to the Y_{ij} element of the admittance matrix Y_{BUS}. In this matrix, the admittance corresponding to the transient reactance of generators is merged with the network admittances. P_{Bi} and Q_{Bi} represent active and reactive power injected to the ith bus.

2.3. PMSG-based wind farm

PMSG-based wind turbines use back-to-back voltage source converters (VSCs). The control strategy of the generator-side converter (GSC) ensures variable speed operation of the PMSG. The grid-side converter controls active and reactive powers delivered to the grid. The above-mentioned characteristics give a particular transient behavior of this generation system compared to traditional synchronous generators. During contingencies, the rotational speed of synchronous generators oscillates as a result of the unbalance between the input mechanical power and produced electrical power. The grid frequency is influenced by rotor speed variations and the inertia of the synchronous generator plays an important role in damping these oscillations. In the case of direct drive wind turbines, the generated electrical power is always synchronized with the grid frequency and can be controlled regardless of speed variations of the PMSG. Hence, the PMSG is electromechanically decoupled from the grid and the wind system is considered with no influence on power system inertia [22]. During faults, PMSG-based wind systems cannot deliver their rated power as a result of the limitations in converter ratings. Taking into account the above performances, the model of the direct drive wind farm is represented by a voltage source behind an equivalent reactance as depicted in Figure 2.

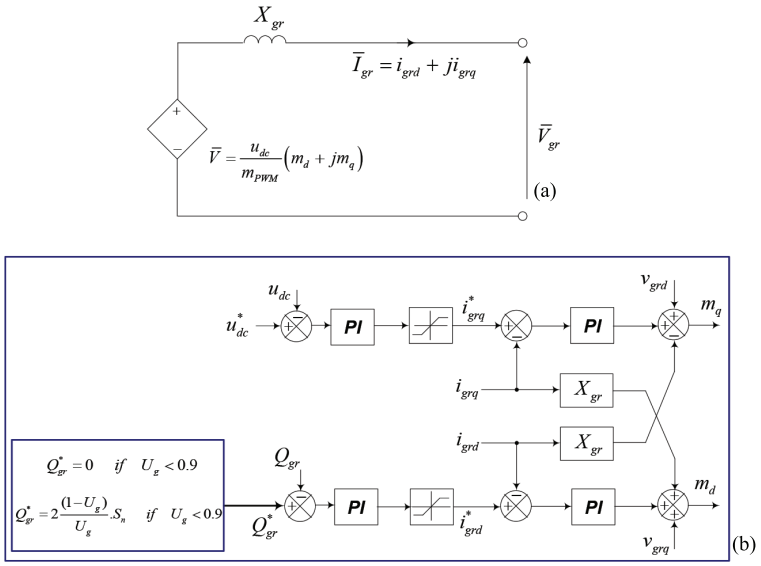

Figure 2. Model and control strategy of the grid-side converter.

The grid side converter is modeled by an averaged model, which only generates fundamental frequency components [23]:

$$v_{d,q} = \frac{u_{dc}}{m_{PWM}} m_{d,q} \tag{8}$$

m_d and m_q are the modulating signals generated by the control block of the grid-side converter. The DC link voltage u_{dc} is maintained constant by controlling the q-axis current and the produced reactive power is controlled in the d-axis component. PI regulators are used to control the grid currents and the two control loops are decoupled by adding feedforward components. A phase locked loop (PLL) is used to find the dq components of the grid voltage. The voltage ripple across the DC link capacitor is calculated by:

$$C_{dc} \cdot \frac{du_{dc}}{dt} = I_{GSC} - \frac{1}{m_{PWM}} (m_d i_{grd} + m_q i_{grq}) \tag{9}$$

The direct drive wind farm is aggregated by a single unit, which is scaled to give the same power production. Assuming a wind farm comprising n wind turbines connected to a common bus, the parameters of the equivalent model are calculated by:

$$C_{dc,e} = n \cdot C_{dc} \tag{10}$$

$$X_{gr,e} = X_{gr}/n \tag{11}$$

3. Control strategies of the PMSG-based wind farm

3.1. Unity power factor

In unity power factor (UPF) control, the reference of reactive power Q^*_{gr} in Figure 2 is set to zero regardless of grid conditions. The wind farm delivers only active power to the grid and the grid current is limited to the rated value I_n [10].

3.2. Reactive power control

Figure 2 shows the typical reactive power control. In this case, the PMSG-based wind system delivers a reactive current to support the grid voltage. The reactive current is proportional to the magnitude of the voltage drop as required by the grid codes. In addition, the delivered current is limited by the current ratings of the grid-side converter (I_n). If a voltage drop is detected, the control strategy of the GSC forces the active power to zero at the PMSG output, and the reactive current delivered to the grid is limited to its maximal value I_n.

3.3. Virtual synchronous machine

VSM is a promising control approach based on controlled power electronic converters. This concept aims to operate distributed generation sources in a similar way as a conventional synchronous generator. It can be used to enhance the stability of the grid during transient events [24]. Figure 3 illustrates the VSM control implemented in a PMSG-based wind turbine. In this figure, the PMSG is connected to the grid via a back-to-back VSC. The detailed virtual synchronous control diagram is depicted in Figure 4. The behavior of the VSM can be modeled by the following swing equation of a traditional SG:

$$\frac{d\omega_{VSM}}{dt} = \frac{P_{mec}}{T_a} - \frac{P_{gr}}{T_a} - \frac{P_d}{T_a} \tag{12}$$

Here, ω_{VSM} is the angular speed of the VSM of the virtual inertia, P_{mec} is the virtual mechanical input power, P_{gr} is the active power delivered to the grid, and P_d is the damping power. T_a is equivalent to $2H$ in a traditional SG. The VSM speed ω_{VSM} can be expressed as a function of the speed deviation $\delta\omega_{VSM}$ and the grid frequency ω_{gr} calculated by the PLL:

$$\omega_{VSM} = \delta\omega_{VSM} + \omega_{gr} \tag{13}$$

The VSM angle is expressed by:

$$\frac{d\theta_{VSM}}{dt} = \omega_{VSM}.\omega_b \tag{14}$$

The damping power can be expressed as a function of the damping coefficient k_d as follows:

$$P_d = k_d\left(\omega_{VSM} - \omega_{gr}\right) \tag{15}$$

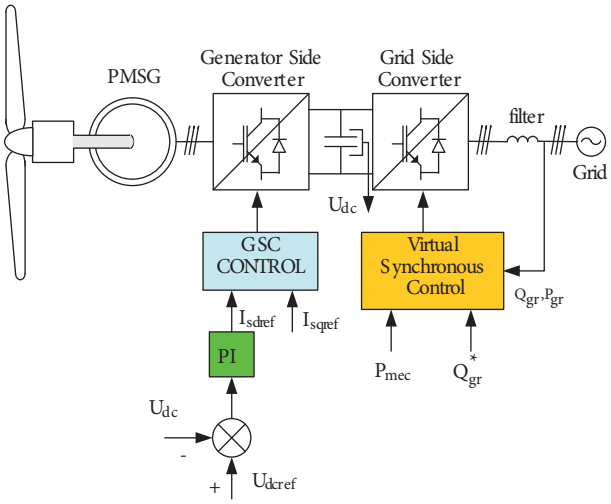

Figure 3. VSM control diagram of PMSG-based wind turbine.

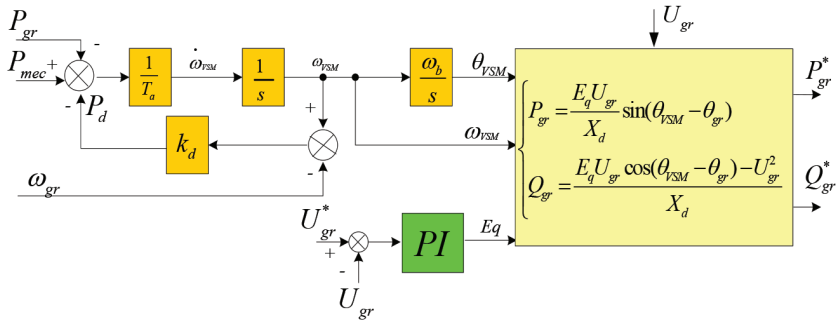

Figure 4. Detailed virtual synchronous control.

4. Trajectory sensitivity analysis

As the generator stator and grid transients are neglected, the power system model results in a set of differential algebraic equations (DAEs) taking the following form: [20]:

$$\dot{x} = f(x, y) \tag{16}$$

$$0 = \begin{bmatrix} g^{-}(x, y, \lambda) & h(x, y, \lambda) < 0 \\ g^{+}(x, y, \lambda) & h(x, y, \lambda) > 0 \end{bmatrix} \tag{17}$$

Here $x(t_0) = x_0$, $y(t_0) = y_0$, and a switching occurs when $h(x, y, \lambda) = 0$. In the above equations, x represents the generator's state variables such as rotor angles, speed deviation, and internal voltages. y is the algebraic variables' vector, which consists of the magnitudes and the angles of bus voltages. λ describes a set of system parameters such as line reactance, load powers, or fault clearing time. Let λ_0 be the nominal value of a specific system parameter λ. The trajectory sensitivities of state variables with respect to small variations of λ_0 are given by [24, 25]:

$$\dot{x}_\lambda = \left[\frac{\partial f}{\partial x}\right] x_\lambda + \left[\frac{\partial f}{\partial y}\right] y_\lambda + \left[\frac{\partial f}{\partial \lambda}\right] \tag{18}$$

$$0 = \left[\frac{\partial g}{\partial x}\right] x_\lambda + \left[\frac{\partial g}{\partial y}\right] y_\lambda + \left[\frac{\partial g}{\partial \lambda}\right] \tag{19}$$

In Eq. (18), $x_\lambda = \partial x/\partial\lambda$ and $y_\lambda = \partial y/\partial\lambda$. The trajectory sensitivities can be obtained by solving Eqs. (16) and (17) simultaneously with Eq. (18) using any numerical method. In this work, the fault clearing time t_{cl} is chosen as the study parameter ($\lambda = t_{cl}$). Afterward, numerical integration of differential equations is used to resolve the sensitivities equation for two values of t_{cl} (say t_{cl1} and t_{cl2}). Hence, two solutions of state variables are obtained, which are referred to as x_1 and x_2. If Δt_{cl} is sufficiently small, the sensitivities of state variables with respect to t_{cl} can be estimated numerically using the following equation [18]:

$$x_\lambda = \frac{x_2 - x_1}{t_{cl2} - t_{cl1}} \tag{20}$$

The sensitivities x_λ are calculated for two values of the fault clearing time, which are assumed to be less than critical time t_{cr}, which induces instability. Extensive experience with power systems shows that sensitivities undergo larger excursions as the clearing time approaches the critical time. Therefore, they can be used as a metric to estimate the transient stability of the proposed power systems. In [26], the authors proposed to use the norm of the sensitivity vector to measure the proximity to instability. This quantity gives information about the equilibrium state of the overall power system. The sensitivity norm of a power system including an m-machine is calculated as:

$$S_N = \sqrt{\sum_{i=1}^{m} \left(\left(\frac{\partial \delta_i}{\partial t_{cl}} - \frac{\partial \delta_j}{\partial t_{cl}} \right)^2 + \left(\frac{\partial \Delta\omega_{r_i}}{\partial t_{cl}} \right)^2 \right)} \tag{21}$$

Here, machine j is selected as the reference. Then the reciprocal norm η is calculated:

$$\eta = \frac{1}{\max(S_N)} \tag{22}$$

As the system approaches instability, the sensitivity terms show higher oscillation and, consequently, the reciprocal norm η tends to zero. Therefore, it is calculated for two or three values of the clearing time t_{cl} and the critical time is estimated using linear interpolation.

5. Impact of wind production on transient stability

The test case power system is depicted in Figure 1. In order to identify the best control strategy, the study was divided into four scenarios. In the first one, the transient stability of the power system is analyzed assuming that all the generated power is delivered by synchronous generators. The synchronous generator connected to bus 8 delivers 20% of the produced power. In the following scenarios, the direct drive wind farm is integrated using three control method, unity power factor (UPF), reactive power control (RPC), and VSM control, to assess its impact on the transient stability of the overall system. The global wind penetration level is kept constant (20%) to identify the best production scenario. In all scenarios, the stability index is calculated by simulating a 3-phase fault occurring in one of the lines of the systems. For the two-area power system, it is assumed that the fault occurs at the line section connecting buses 3 and 4. Faults are considered to take place at distances of 10 km, 50 km, and 90 km from bus 4. The simulation starts from the steady-state condition, which is run for a small time. Then the fault is applied and the system behavior is simulated for a longer time

(approximately 3 s), and the trajectory of state variables is recorded. The simulation is run once again with a small variation in the fault clearance time. The considered fault durations are 0.25 s, 0.35 s, and 0.45 s. The results are presented in the following.

Scenario 1: Synchronous generator

In this scenario, only synchronous generators are considered. Synchronous generator production is equal to 700 MW and 370 MW respectively for generators G1 and G2. The production of the added SG G3 is assumed equal to 290 MW. The values of η for different fault locations are listed in Table 2. It is observed that the reciprocal norm η decreases when the fault duration is increased, regardless of the fault position. This result is in accordance with the analysis performed in Section 4, and it shows that trajectory sensitivity analysis represents a reliable measure of stability. It is also noticed that the critical time decreases when the fault location goes closer to connection bus 8.

Table 2. Values of η_0 for different fault locations without the integration of the direct drive wind system.

	Values of η_0			
Fault Location	Fault clearing time			Estimated critical time
	0.25 s	0.35 s	0.45 s	
10 km	2.49	1.93	1.55	0.77
50 km	2.73	2.21	1.95	0.93
90 km	2.34	2.04	1.86	1.22

Generator behavior during a three-phase fault is depicted in Figure 5a. It is observed that the disturbing event causes oscillations of all variables. It can be seen that all rotor speeds increase from 50 Hz to a value around 50.5 Hz. Rotor speeds of G1 and G2 remain in the normal operating range (49.5–50.5 Hz), while the rotor speed of G3 slightly exceeds this range. The fault also gives rise to subtransient oscillations of active and reactive power of G2 and G3. After the fault clearance, the produced powers continue to oscillate during a transient period of 1.5 s before reaching a fixed value (0.5 p.u).

Scenario 2: Transient stability with the PMSG-based wind farm (UPF)

In this scenario, the PMSG-based wind system is operated at unity power factor regardless of network conditions ($Q^*_{gr} = 0$). It is observed that the reciprocal norm decreases compared to the values of Table 2, regardless of fault location or duration. Consequently, the integration of the wind system deteriorates the stability of the power system. Indeed, the power produced by the wind farm is electromechanically decoupled from the grid and it does not contribute to the power system inertia [6]. Thus, synchronous generators will experience higher changes in rotor speeds during disturbances as depicted in Figure 5b. The rotor speeds of G1 and G2 exceed the limit of 50.5 Hz. Active and reactive powers produced by the wind farm go back to their initial values after the fault clearance due to the action of current control loops.

Scenario 3: Transient stability with the PMSG-based wind farm (RPC)

In this scenario, CCTs are found equal to 1.12 s, 1.38 s, and 0.72 s, respectively, for distances of 10, 50, and 90 km. The obtained CCTs are higher than in the previous scenario, which uses UPF control. This result confirms the importance of injecting reactive power to support the grid voltage. Figure 5c shows the rotor speed of the synchronous generators. When reactive power is injected into the grid, the power system shows a higher ability to keep synchronism between the interconnected synchronous generators.

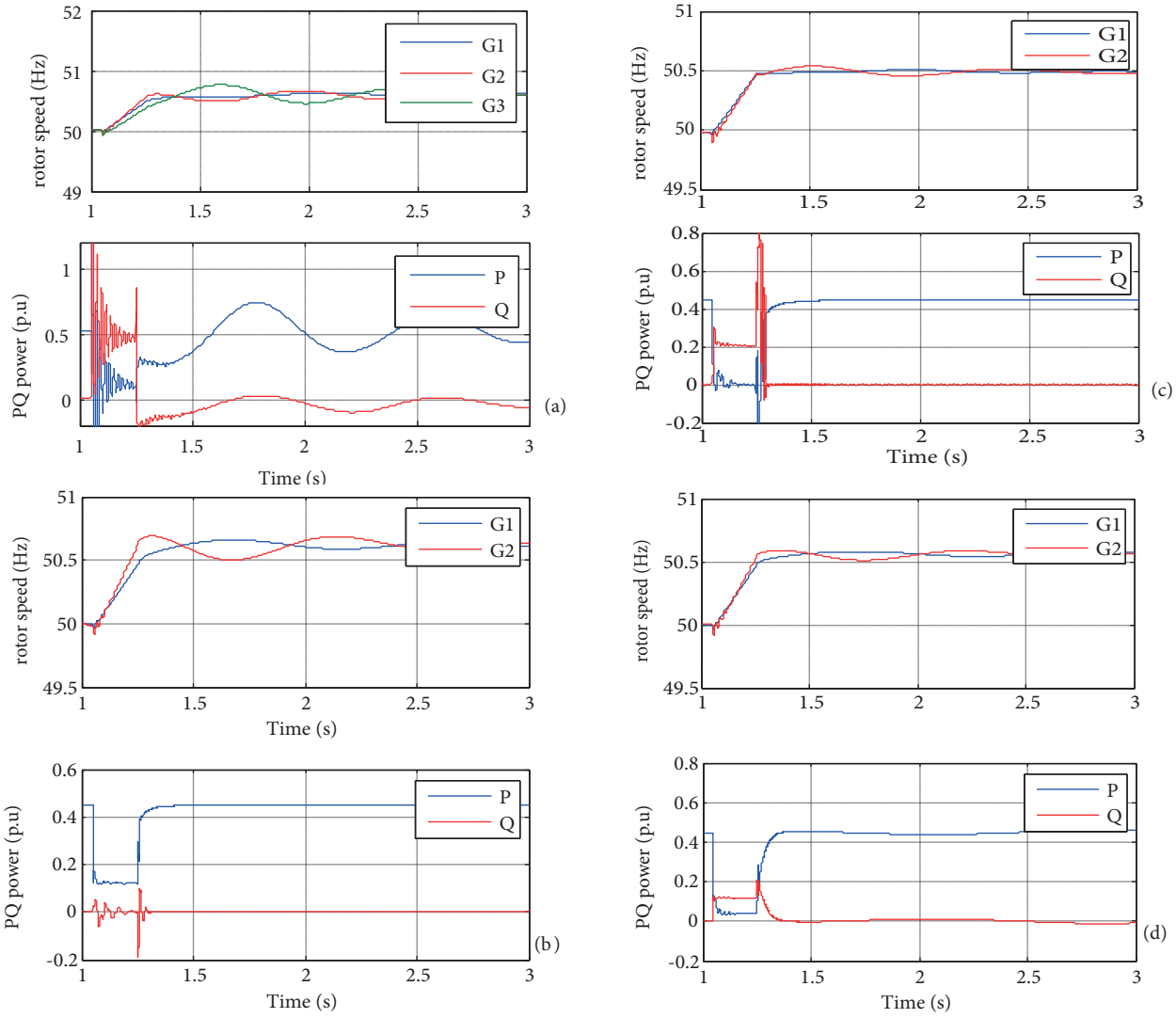

Figure 5. Generator behavior, rotor speeds of synchronous generators, and active and reactive powers delivered by bus 8 generation system during a three-phase fault: (a) Scenario 1, (b) Scenario 2, (c) Scenario 3, (d) Scenario 4.

Scenario 4: Transient stability with the PMSG-based wind farm (VSM)

In this scenario, the performances of VSM control are investigated. Figure 5d shows the rotor speeds of G1 and G2, which exceed the limit value of 50.5 Hz. It is noted that VSM control performs better than UPF control in terms of smoothing the oscillations of rotor speeds.

Figure 6 summarizes the obtained critical times for the above-mentioned scenarios. When the fault location is close to the bus of common connection (10 km), the direct drive technology with RPC gives higher critical time (1.12 s), followed by the VSM control and finally the UPF control. For distant fault locations (90 km), the synchronous generator gives a better stability level (1.45 s). The stability level with RPC (0.72 s) is close to the stability level with VSM control (0.8 s). By comparing the above results, it is noted that the best control strategy for the variable speed wind system consists of using the full power of the grid-side converter to support the grid voltage with reactive power injection. Therefore, it is important to improve the transient

performances of the VSM control in order to go as much as possible up to the behavior of real synchronous generators during faults.

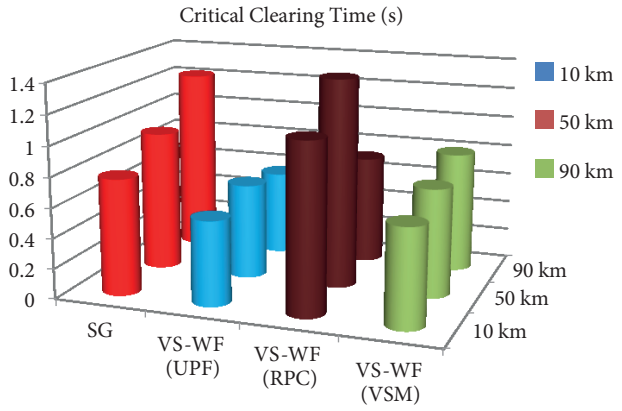

Figure 6. CCT of the different scenarios as a function of fault locations.

6. Improved VSM control of PMSG-based wind farms

From the previous analysis, it is concluded that RPC gives the best level of stability, followed by the VSM control. The objective of this section is to improve the transient performances of the VSM control strategy. It is proposed to calculate the reference powers P_{gr}^{*} and Q_{gr}^{*} delivered by the VSM (Figure 4) based on the transient model of the synchronous generator rather than the steady-state equations [21]. This model adopts the quasi-sinusoidal approximation; that is, the stator terms $\frac{d\psi_s}{dt}$ are omitted in Park's equations of the grid-connected synchronous generators. With this assumption, the stator voltages in the per unit system are given by:

$$u_{gd} = -\psi_{sq} - R_s \cdot i_{gd} \tag{23}$$

$$u_{gq} = \psi_{sd} - R_s \cdot i_{gq} \tag{24}$$

u_{gd} and u_{gq} are the dq components of the grid voltage $\bar{U}_g$. During transients, the variation of the rotor speed with respect to the nominal speed is relatively small and its effect on stator voltages remains insignificant. Thus, in the above equations, $\omega_r \approx 1$. In addition, the effect of dampers is neglected. The flux equations are given by:

$$\psi_{sd} = -X_d i_{gd} + X_{sd} i_{fd} \tag{25}$$

$$\psi_{sq} = -X_q i_{gq} \tag{26}$$

$$\psi_{fd} = X_{ffd} \cdot i_{fd} - X_{sd} i_{gd} \tag{27}$$

Here, X_d and X_q are respectively the d-axis and q-axis reactance, X_{sd} represents the d-axis mutual inductance between the stator and the rotor windings, and X_{ffd} is the self inductance of the field circuit. The rotor circuit voltage equation is written as follows:

$$\frac{1}{\omega_b}\frac{d\psi_{fd}}{dt} = v_{fd} - R_f \cdot i_{fd} \tag{28}$$

Generally, the above equations are written as a function of $E_q^t = \frac{X_{sd}}{X_{ffd}}\psi_{fd}$ and $E_{fd} = \frac{X_{sd}}{R_f}v_{fd}$ [21, 22]. Eq. (28) becomes:

$$\frac{dE_q^t}{dt} = \frac{\omega_b R_f}{X_{ffd}}E_{fd} - \frac{\omega_{ro}X_{sd}}{X_{ffd}}R_f \cdot i_{fd} \tag{29}$$

By introducing E_q^t in Eq. (27), it becomes:

$$E_q^t = X_{sd}i_{fd} - \frac{X_{sd}^2}{X_{ffd}}i_{gd} \tag{30}$$

The transient inductance along axis d is defined by [24]:

$$X_d^t = X_d - \frac{X_{sd}^2}{X_{ffd}} \tag{31}$$

By inserting Eqs. (31)and (30) into Eq. (29), the rotor winding equation becomes:

$$\frac{dE_q^t}{dt} = \frac{1}{T_{d0}^t}\left(E_{fd} - E_q^t - \left(X_d - X_d^t\right)i_{gd}\right) \tag{32}$$

$T_{d0}^t = \frac{X_{ffd}}{\omega_{ro}R_f} = \frac{X_{fd}+X_{sd}}{\omega_{ro}R_f}$ is the open-circuit time constant of the rotor. Neglecting the resistance R_s, and inserting Eqs. (25) and (31) into Eq. (24), the following expression of current i_{gd} is obtained:

$$i_{gd} = \frac{E_q^t - u_{gq}}{X_d^t} \tag{33}$$

Then the differential equations of the VSM in the dq frame are expressed as follows:

$$\frac{d\theta_{VSM}}{dt} = \omega_{VSM}.\omega_b \tag{34}$$

$$\frac{d\omega_{VSM}}{dt} = \frac{1}{2H}\left(-k_d\left(\omega_{VSM} - \omega_{gr}\right) + P_{mec} - P_{gr}\right) \tag{35}$$

$$T_{d0}^t\frac{dE_q^t}{dt} = -\frac{X_d}{X_d^t}E_q^t + \left(\frac{X_d}{X_d^t} - 1\right)U_g cos\left(\theta_{VSM} - \theta_{gr}\right) + E_{fd} \tag{36}$$

This model is implemented to achieve the VSM control of the PMSG-based wind farm as presented in Figure 4. Active and reactive power references delivered by the VSM are calculated based on this transient model:

$$P_{gr}^* = \frac{E_q^t}{X_d^t}U_g \sin\left(\theta_{VSM} - \theta_g\right) + 0.5\left(\frac{1}{X_q} - \frac{1}{X_d^t}\right)U_g^2 \sin\left(2(\theta_{VSM} - \theta_g)\right) \tag{37}$$

$$Q_{gr}^* = \frac{E_q^t}{X_d^t}U_g cos(\theta_{VSM} - \theta_g) + 0.5{U_g}^2\left(\frac{1}{X_q} - \frac{1}{X_d^t}\right)\cos\left(2(\theta_{VSM} - \theta_g)\right) + 0.5\frac{1}{X_q}{U_g}^2\left(\frac{1}{X^t{}_d} - \frac{1}{X_q}\right) \tag{38}$$

Figure 7a shows active and reactive power references P^*_{gr} and Q^*_{gr} as a function of the internal angle of the VSM when the steady-state equations are used. It is noted that, when the grid voltage drops to 10 % of the rated value, the active power decreases to a value around 0.05 p.u. for the given point of operation. For the reactive power Q^*_{gr}, it increases from 0 to 0.08 p.u. Hence, the wind farm does not effectively support the grid voltage. Figure 7b illustrates the delivered active and reactive powers when the VSM uses the transient model of the synchronous generator. During the voltage dip, the reference reactive power increases to 0.3 p.u. This value is significantly higher than in the previous case, which means that improved VSM control can efficiently support the grid voltage and improve the stability level of the power system.

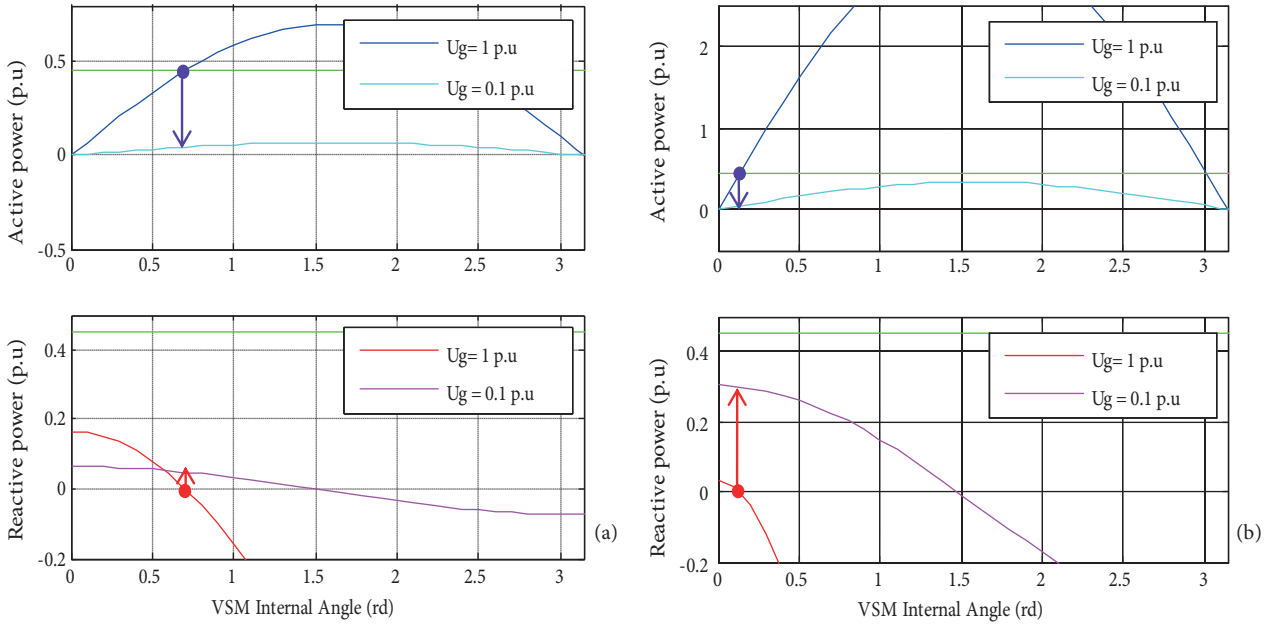

Figure 7. Power references delivered by VSM as a function of the virtual internal angle ($P_{mec} = 0.45$p.u): (a) classical model, (b) improved VSM model.

To verify the advantages of the improved VSM control, two operating points of the power system were considered as depicted in Figure 8. Generator behaviors were simulated assuming a three-phase fault that occurs at a distance of 10 km from bus 4. In the first case, the PMSG-based wind farm is assumed to produce 20% of the total generated power. Figure 8a depicts the active and reactive powers delivered to the grid when the classical and the improved VSM are used. When the fault occurs, the active power delivered by the IVSM control equals the average power delivered by the SG and it injects more than 0.5 p.u. of reactive power while the classical VSM control injects less than the half of this value. During the postfault period, power oscillations with the improved VSM are close to the transient response of the SG, whereas subtransient oscillations are removed. With the classical VSM, the produced powers are constant and they return gradually to their initial values. In the second scenario (Figure 8b), the penetration rate of the wind power was increased to 31%. Again, it is observed that the «PQ» power produced with the improved VSM is almost equal to the average power produced by the SG. The wind farm supports the grid voltage with a reactive power production of 0.45 while the classical VSM gives only 0.2 p.u. In the moments subsequent to the fault, active and reactive powers are almost equal to the power produced by the SG. However, for the classical VSM, the reactive power takes a negative value, which means that the wind farm does not provide primary voltage control. Hence, with the

improved VSM control, the wind farm supports the grid voltage more efficiently and it behaves more and more like conventional power plants.

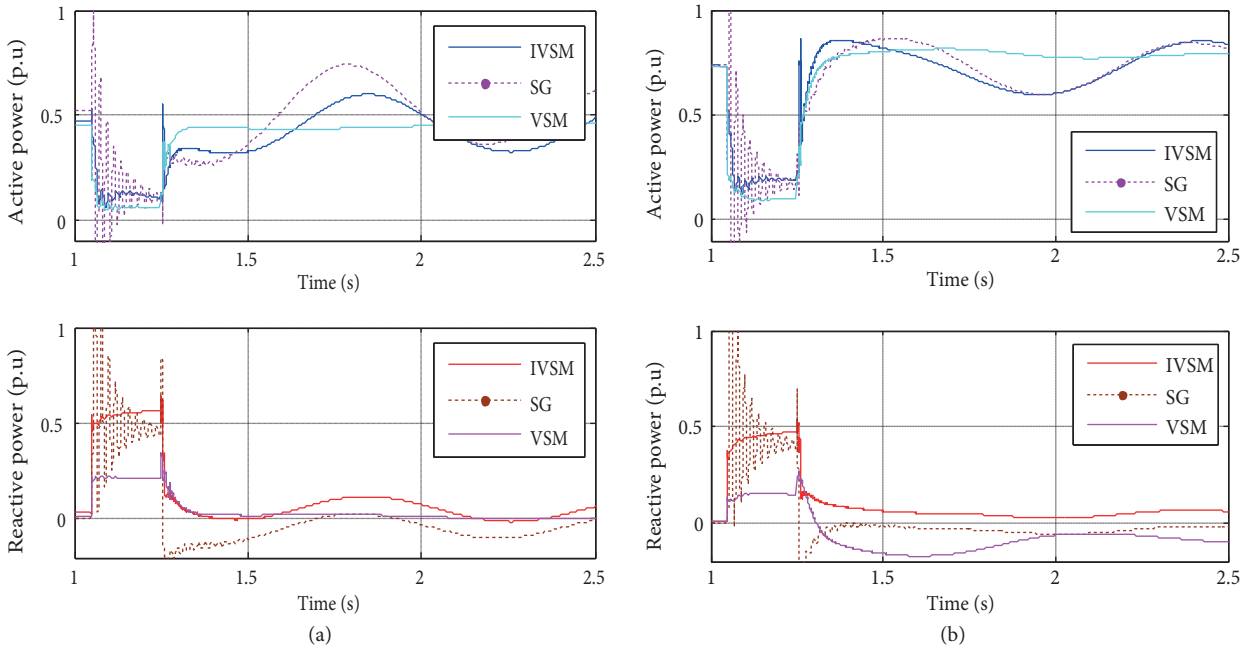

Figure 8. Active and reactive powers delivered to the grid by the SG and the PMSG-based wind farm with the two VSM controls in the event of a three-phase fault: (a) 20% penetration rate, (b) 31% penetration rate.

In order to evaluate the impact of this solution on the overall stability level of the power system, the CCTs were calculated for the two production patterns (20% and 31% penetration rate) and for different fault locations (Figure 9). For the first case (Figure 9a), it is noted that the improved VSM gives the highest value of the CCTs (0.8 s for 10 km, 1.19 s for 50 km, and 1.78 s for 90 km), followed by the SG (0.79 s for 10 km, 0.88 s for 50 km, and 1.2 s for 90 km). The stability level is significantly affected when the penetration rate of wind power is increased to 31%, as depicted in Figure 9b. The CCTs drop around 0.54–0.64 s for the two control strategies; however, the improved VSM control gives the highest values. Thus, it is concluded that with the improved VSM control, the power system attains a good level of stability compared to the classical VSM.

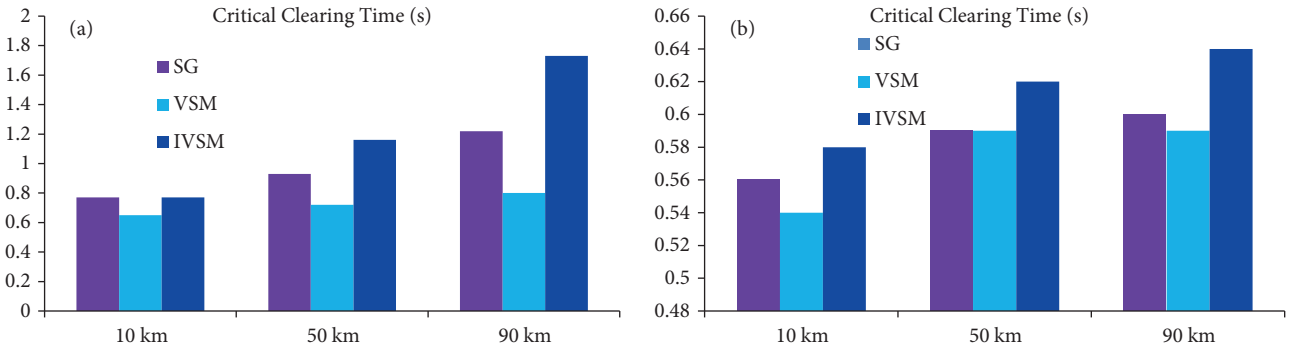

Figure 9. CCTs given by the SG, VSM, and IVSM as functions of fault locations: (a) with a penetration rate of 20%, (b) with a penetration rate of 31%.

7. Conclusion

In this paper, the impact of PMSG-based wind farms using different control modes on power system transient stability was analyzed. First, the power system and the direct drive wind system were modeled. Using the trajectory sensitivity approach, the critical clearing time in a variety of production scenarios was calculated. By considering the CCT as a stability index, the transient stability of the power system was analyzed assuming a wind power penetration rate of approximately 20%. It was found that RPC gives the best transient stability level, followed by the classical VSM control. Hence, an improved VSM control was proposed based on the transient model of SGs. The proposed method has given excellent results in terms of transient stability improvement compared to the classical model of the VSM control.

References

[1] IRENA. Renewable Capacity Statistics 2017. Abu Dhabi, UAE: International Renewable Energy Agency, 2017.

[2] Zhi W, Shien H. Comparative analysis on critical clearing time of power system connected with large wind farm. In: International Conference on Advanced Power System Automation and Protection; 2011; Beijing, China.

[3] Gounder Y, Nanjundappan D, Boominathan V. Enhancement of transient stability of distribution system with SCIG and DFIG based wind farms using STATCOM. IET Renew Power Gen 2016; 10: 1171-1180.

[4] Akhmatov V. System stability of large wind power networks: a Danish study case. Int J Elec Power 2005; 28: 48-57.

[5] Moradzadeh M, Shayeghi H, Vandevelde L, Saif M. Impact of increased penetration of large-scale wind farms on power system dynamic stability - a review. In: IEEE 15th International Conference on Environment and Electrical Engineering; 2015; Rome, Italy.

[6] Liu S, Li G, Zhou M. Power system transient stability analysis with integration of DFIGs based on center of inertia. CSEE Journal of Power and Energy Systems 2016; 2: 1120-1121.

[7] Gautam D, Vittal V, Harbour T. Impact of increased penetration of DFIG-based wind turbine generators on transient and small signal stability of power systems. IEEE T Power Syst 2009; 24: 1426-1434.

[8] Vittal E, O'Malley M, Keane A. Rotor angle stability with high penetrations of wind generation. IEEE T Power Syst 2012; 27:353-362.

[9] Mitra A, Chatterjee D. A new sensitivity based approach to study the impact of wind power penetration on transient stability. In: IEEE International Conference on Power Electronics, Drives and Energy Systems; 2012; Bengaluru, India.

[10] Liu Z, Liu C, Li G, Liu Y, Liu Y. Impact study of PMSG-based wind power penetration on power system transient stability using EEAC theory. Energies 2015; 8: 13419-13441.

[11] Shang L, Hu J, Yuan X, Chi Y. Understanding inertial response of variable-speed wind turbines by defined internal potential vector. Energies 2017; 10: 22.

[12] Driesen J, Visscher K. Virtual synchronous generators. In: IEEE Power and Energy Society General Meeting; 2008; Pittsburgh, PA, USA.

[13] Mathisen ER. Application of virtual synchronous machines for integration of offshore wind turbines into the power system of offshore oil and gas platforms. PhD, Norwegian University of Science and Technology, Trondheim, Norway, 2016.

[14] Jaber A, Yushi M, Toshifumi I. Power system stabilization using virtual synchronous generator with alternating moment of inertia. IEEE J Em Sel Top C 2015; 3: 451-458.

[15] Yi W, Jianhhui M, Xiangyu Z, Lie X. Control of PMSG-based wind turbines for system inertial response and power oscillation damping. IEEE T Sustain Energ 2015; 6: 565-574.

[16] Yiwei M, Wenchao C, Liu Y, Fred W, Leon MT. Virtual synchronous generator control of full converter wind turbines with short term energy storage. IEEE T Ind Electron 2017; 64: 8821-8831.

[17] Chatterjee D, Ghosh A. Improvement of transient stability of power systems with STATCOM-controller using trajectory sensitivity. Int J Elec Power 2011; 33: 531-539.

[18] Nasri A, Eriksson R, Ghandhari M. Using trajectory sensitivity analyses to find suitable locations of series compensators for improving rotor angle stability. Electr Pow Syst Res 2014; 2; 1-8.

[19] Padyar K. Power System Dynamics Stability and Control. Delhi, India: C Publications, 2008.

[20] Sauer PW, Pai MA. Power System Dynamics and Stability. Upper Saddle River, NJ, USA: Prentice Hall, 1998.

[21] Kundur P. Power System Stability and Control. New York, NY, USA: McGraw-Hill, 1994.

[22] Hao ZH, Yu YX, Zeng Y. Transient performance of DFIG power angle in wind farm and its control strategy. Electr Power Aut Equi 2011; 31: 79–83.

[23] Irevani R, Yazdani A. Voltage Sourced-Converter in Power System. Modeling, Control and Application. Hoboken, NJ, USA: Wiley, 2010.

[24] D'Arco S, Are Suul J, Fosso OB. A virtual synchronous machine implementation for distributed control of power converters in SmartGrids. Electr Pow Syst Res 2015; 122: 180-197.

[25] Pai MA, Nguyen TB. Trajectory sensitivity theory in nonlinear dynamical systems: some power system applications. In: Derong L, Panos JA, editors. Stability and Control of Dynamical Systems with Applications. Boston, MA, USA: Birkhauser, 2003, pp. 271-292.

[26] Laufenberg MJ, Pai MA. A new approach to dynamic security assessment using trajectory sensitivities. IEEE T Power Syst 1998; 13: 953–958.